Ultrafast above-threshold dynamics in the radical anion of a prototypical quinone electron acceptor

Daniel A. Horke,[§†] Quansong Li,[*‡] Lluís Blancafort[‡] and Jan R. R. Verlet[†]

[†]*Department of Chemistry, University of Durham, Durham DH1 3LE, United Kingdom*
[‡]*Institut de Química Computacional i Catàlisi and Departament de Química, Universitat de Girona, Campus de Montilivi, 17071 Girona, Spain.*

Quinones feature prominently as electron acceptors in nature. Their electron transfer reactions are often highly exergonic, for which Marcus theory predicts reduced electron transfer rates because of a free energy barrier occurring in the inverted region. However, the electron transfer kinetics involving quinones can appear barrierless. Here, we consider the intrinsic properties of the para-benzoquinone radical anion, which serves as the prototypical electron transfer reaction product involving a quinone-based acceptor. Using time-resolved photoelectron spectroscopy and *ab initio* calculations, we show that excitation at 400 and 480 nm yields excited states that are unbound with respect to electron loss. These excited states are shown to decay on a sub-40 fs timescale through a series of conical intersections with lower-lying excited states, ultimately forming the ground anionic state and avoiding autodetachment. From an isolated electron acceptor perspective, this ultrafast stabilisation mechanism accounts for the ability of para-benzoquinone to capture and retain electrons.

[§] Current address: Center for Free-Electron Laser Science, DESY, Notkestr. 85, 22607 Hamburg, Germany
[*] Current address: Key Laboratory of Cluster Science of Ministry of Education, School of Chemistry, Beijing Institute of Technology, 100081 Beijing, China

Quinones are found throughout nature as key electron acceptor intermediates,[1,2] with examples including plastoquinone which is involved in the electron transfer chain of photosystem II, and ubiquinone (coenzyme Q10) which plays a key role in aerobic cellular respiration.[3] The central moiety responsible for the electron accepting ability in quinones is para-benzoquinone (pBQ), shown in Figure 1c. Electron transfer reactions involving pBQ can be highly exergonic and are therefore often classed as being in the Marcus inverted region. [4-10] This is shown schematically by the green path in Figure 1a, where a barrier between the Gibbs free energy of the reactants and products lowers the rates of the electron transfer process. However, even in the earliest experimental verifications of the inverted region for intramolecular electron transfer, several electron acceptors based on pBQ showed marked deviations from the expected behaviour, with transfer rates approaching those of a barrierless reaction. [11] It has been proposed that such deviations may involve electronically excited states of the product radical anion of para-benzoquinone (pBQ•$^-$),[12] which could provide reaction pathways that bypass the barrier, as shown in Figure 1a with purple arrows. [6,13-17] At present, very little is known about the excited state dynamics of pBQ•$^-$ and, more generally, most radical ions. Here, we take a bottom-up view of electron transfer and consider what happens to the excited states that are initially formed following electron capture by an isolated pBQ molecule. Gaining a fundamental understanding of the intrinsic dynamics of pBQ•$^-$ is a key step to developing a comprehensive picture of electron transfer processes involving quinones.

We approach the above problem using a combination of time-resolved gas-phase spectroscopy and high-level *ab initio* calculations. Gas-phase[12,18-20] and computational[21-24] studies have already provided tantalising glimpses of the remarkable nature of pBQ as an electron acceptor. pBQ is planar both as a neutral and radical anion with D_{2h} symmetry and has ground states of ^1A_g and $^2B_{2g}$ symmetry, respectively. pBQ has an electron affinity of 1.86 eV. [12,25] Electron attachment spectra using the scavenger method showed resonances at

0.7 eV and 1.35 eV in pBQ that led to the formation of pBQ•⁻ with lifetimes of several μs. [26-28] Photodetachment spectroscopy of pBQ•⁻ revealed the nature of a number of these resonances in the detachment continuum. [12] Specifically, at 2.50 eV an intense and broad resonance was assigned to the origin of the ^2A_u state, while a series of weaker narrow resonances was assigned to vibrational levels of two lower lying nπ* states ($^2B_{2u}$ and $^2B_{3g}$) that are optically dark. The energy level diagram in Figure 1b shows the location of these resonances.

From the point of view of an electron approaching pBQ, these anionic resonances in the detachment continuum can capture an electron. Subsequent formation of the anionic ground state through internal conversion would redistribute the excess internal energy amongst all the vibrational modes. In a condensed-phase environment, this energy will be quenched by the surroundings. However, the initially formed excited states of pBQ•⁻ can be unbound with respect to electron loss. For the above picture to be feasible, internal conversion must be able to compete with autodetachment. Electron attachment spectra suggest that it can, [26-28] but how does this occur given that these resonances are in some cases > 1 eV above the detachment threshold?

In order to gain a fundamental understanding of the processes involved following electron capture, it is necessary to observe the relaxation dynamics in real time. This is achieved here by using time-resolved photoelectron (PE) spectroscopy on photoexcited pBQ•⁻.[29,30] Although photoexcitation is not the same as electron attachment, the initial photoexcited state may be expected to closely resemble the initially populated resonance following electron impact and the subsequent relaxation dynamics will generally be comparable for both processes. Hence, time-resolved PE spectroscopy is well suited to observe the electronic dynamics in such systems. We use *ab initio* calculations to support our

results, which together provide a detailed picture of the mechanism by which internal conversion proceeds.

Results and Discussion

Electronic structure and dynamics

The electronic structure of pBQ•$^-$ has been considered with CASPT2//CASSCF calculations (CASPT2 energies at CASSCF optimized structures). We use the ionisation potential-electron affinity (IPEA) shift that reduces systematic errors of the CASPT2 method.[31] The results are summarised in Table 1. At this level of theory, the adiabatic electron affinity is 2.04 eV and the ^2A_u state is calculated at 2.58 eV, which are in good agreement with the experimental values of 1.86 eV and 2.50 eV, respectively.[12] Dominant electronic configurations given in the footnote refer to the orbitals displayed in Figure 1e. We consider only the energies and structures of the five lowest states, with an excitation energy below 3.2 eV at the minimum geometry of the $^2B_{2g}$ state. The first entry of Table 1 gives the vertical excitation energies of the anion, with the oscillator strengths in brackets.

Experimentally, we excite pBQ•$^-$ at 2.58 eV (480 nm) and 3.10 eV (400 nm), which is close to the resonances at 0.7 eV and 1.35 eV above threshold. [26-28] Our calculations agree with the assignment of the former to the ^2A_u state involving the excitation of the unpaired electron from the $2b_{2g}$ to the $1a_u$ orbital ($2b_{2g}\rightarrow 1a_u$). The 3.10 eV excitation mainly populates the $^2B_{3u}$ state, the wave function of which is dominated by an excitation corresponding to a Feshbach- resonance ($2b_{3u}\rightarrow 2b_{2g}$), which has a weight of 63%. A significant contribution (15%) also comes from an excitation ($2b_{2g}\rightarrow 3b_{3u}$) that corresponds to a shape-resonance.

The PE spectra taken at photon energies of 2.58 eV and 3.10 eV are shown in Figure 1d. The PE spectrum at 2.58 eV is consistent with the PE spectrum taken at 4.66 eV by Fu *et. al.*[25] (see Figure S1) and the observed feature extending to an electron kinetic energy (*eKE*)

of 0.72 eV corresponds to the $^1A_g + e^-$ detachment channel. Because the excitation pulse is resonant with the $^2A_u \leftarrow {}^2B_{2g}$ transition, this feature contains contributions from direct detachment and autodetachment into the $^1A_g + e^-$ continuum. Near zero *eKE*, an additional peak is observed. In anion PE spectroscopy, and particularly for molecular anions without a permanent dipole moment, the cross-section for electron detachment vanishes at threshold. [32,33] Consequently, these electrons at *eKE* ~ 0 must arise through indirect processes. The appearance of the sharp zero *eKE* feature is typical of that expected for thermionic emission[34-36] and suggests that the ^2A_u can undergo internal conversion to generate vibrationally hot ground state pBQ•$^-$. This can subsequently loose an electron in a statistical fashion. The observation of thermionic emission agrees well with the long lifetime observed following electron attachment to pBQ through this resonance. [26-28]

The appearance of the PE spectrum at 3.10 eV is unexpected. The feature extending to 1.24 eV can be assigned to the $^1A_g + e^-$ detachment channel, as for the 2.58 eV PE spectrum. However, the feature centred at ~0.4 eV, marked by an asterisk, does not appear in the 4.66 eV PE spectrum.[25] Our calculations show that 3.10 eV is resonant with the $^2B_{3u} \leftarrow {}^2B_{2g}$ transition. If we assume that the $^2B_{3u}$ can decay to the ^2A_u state before it can autodetach, then the feature at ~0.4 eV can be assigned to autodetachment from the ^2A_u state. Indeed, the PE spectrum from the ^2A_u state (*i.e.* at 2.58 eV) matches the additional feature in the 3.10 eV PE spectrum, as indicated in Figure 1c. The close resemblance points to the conservation of vibrational energy in the autodetachment process. This is a common propensity rule in PE spectroscopy. Our calculations indicate that the ^2A_u state is a shape-resonance such that autodetachment may be expected to be very fast, thus upholding the propensity to conserve vibrational energy.

The above PE spectra therefore suggest that, upon excitation of the $^2B_{3u}$ state, the system can undergo internal conversion to access the ground state of pBQ•$^-$, despite the fact

that the initial excitation is more than 1.2 eV above threshold. To explore the feasibility of this decay pathway, we have performed time-resolved PE spectroscopy by exciting the $^2B_{3u}$ state at 3.10 eV and probing the subsequent dynamics using a delayed 1.55 eV probe pulse (see excitation scheme in Figure 1b). Figure 2a shows two representative PE spectra at $t = 0$ (pump and probe overlapped in time) and $t < 0$ (probe arrives before pump). An additional feature (highlighted in the inset of Figure 2a) can be discerned at higher *eKE*, while the feature at ~0.4 eV is depleted. The total integrated signal over these features (Figure 2b) shows that: (i) the decay of the high energy feature is mirrored by the recovery of the depleted peak; and (ii) the dynamics occur on a time-scale of <40 fs, limited by our temporal resolution. The pump-probe feature is very similar in appearance to the 3.10 eV PE spectrum, but blue-shifted by 1.55 eV (*i.e.* the probe photon energy). Above, we assigned the bimodal distribution to autodetachment from the $^2B_{3u}$ state at higher *eKE* and from the ^2A_u state at lower *eKE*, following its population via internal conversion. Hence, the dynamics of the individual excited states can be discerned by analysing the high and low *eKE* components of the pump-probe feature separately. Crudely dissecting the pump-probe feature into spectral windows ranging from $1.2 < eKE < 2.0$ and $2.0 < eKE < 3.0$, the time-varying integrated PE signal for both the ^2A_u and $^2B_{3u}$ are shown in Figure 2c. These reveal that there is a clear temporal delay of ~ 20 fs in the appearance of the ^2A_u signal relative to that arising from the $^2B_{3u}$ state, which can be attributed to the timescale of internal conversion from the $^2B_{3u}$ to the lower lying ^2A_u.

Decay mechanism

To gain a mechanistic picture of the dynamics following 3.10 eV excitation, key points along the excited state minimum energy paths have been calculated and these are summarised in Table 1. Figure 3a shows schematic 1D cuts of the relevant potential energy surfaces. Initial excitation from the $^2B_{2g}$ anionic ground state forms the $^2B_{3u}$ excited state. The

primary motion on this state involves totally symmetric stretches of the C=O and C=C bonds, of a_g symmetry. The minimum of the $^2B_{3u}$ state is almost coincident with a conical intersection via which population can be transferred into the lower-lying ^2A_u state (energy difference < 0.1 eV, see Table 1). The transfer is favoured by the fact that the gradient difference vector that funnels population from one state to the other[37-40] has a similar direction as the initial decay coordinate (see vector in Figure 3b). One may expect a weak coupling between the two states because their predominant electronic configurations differ by more than one electron.[41] However, the significant shape-resonance character in the $^2B_{3u}$ state increases the coupling and the calculated interstate coupling is of intermediate strength (see Supplementary section S3). The observed dynamics are consistent with this picture and indicate that decay to the ^2A_u state occurs on a ~20 fs timescale.

Once on the ^2A_u excited state, the system is still metastable with respect to electron loss and is therefore susceptible to autodetachment. Despite this, some fraction of the ^2A_u population can access the ground state as both the 2.58 eV and 3.10 eV PE spectra exhibit clear signatures of thermionic emission, which is necessarily reliant on internal conversion from the ^2A_u state. [34] From the conical intersection between the $^2B_{3u}$ and ^2A_u states, the system propagates towards the minimum energy along the ^2A_u state. The nuclear motion associated with this involves the same modes (C=O and C=C stretches) as those on the $^2B_{3u}$ state. At the ^2A_u minimum, the $^2B_{2u}$ state lies only 0.13 eV higher in energy and the two are therefore very near to an intersection. Similar to the $^2B_{3u}/^2A_u$ case, the gradient difference vector is dominated by the C=O and C=C stretches (see Figure 3c), and the calculated interstate coupling between the ^2A_u and $^2B_{2u}$ states is of intermediate strength (see Supplementary section S3.1). It is more than an order of magnitude larger than that for the other nearby $n\pi^*$ ($^2B_{3g}$) state, which must also intersect the ^2A_u state in the vicinity of its minimum. Hence, we predict that the $^2B_{2u}$ state is populated from the ^2A_u state, although we

cannot conclusively rule out dynamics involving the $^2B_{3g}$ state. The nπ* states cannot be detected in the current experiment because the cross-section to forming the ^1A_g ground state upon photodetachment is likely to be very small as the removal of an electron from these correlates to excited states of the neutral and these are energetically inaccessible.

The motion towards the minimum on the $^2B_{2u}$ state again involves a symmetric stretching mode, predominantly of the C=O bonds. The minimum of the $^2B_{2u}$ state has a relative energy of 2.03 eV. At that structure, the potential energy of the neutral ^1A_g ground state is higher (2.73 eV) and the anion becomes bound. From here, the system can decay further to the ground $^2B_{2g}$ state, which may involve the close-lying $^2B_{3g}$ state as an intermediate. Ultimately, the radical anion will undergo intramolecular vibrational redistribution, and loose the electron statistically through thermionic emission, as is observed in the experiment.

Additional energetically accessible intersections of the $^2B_{3u}$ and ^2A_u states with the $^2B_{2g}$ ground state have also been found and are included in Figure 3a for completeness. Both involve large out-of-plane vibrational modes. The excitation of such modes would require significant intramolecular vibrational redistribution on the $^2B_{3u}$ or ^2A_u states, which we anticipate will occur on a significantly longer timescale than that observed experimentally. Therefore these intersections will most likely not participate in the decay dynamics.

The mechanistic picture inferred from experiment and calculations indicates extremely fast and efficient internal conversion. The *observed* lifetimes for both the $^2B_{3u}$ and ^2A_u states are sub-40 fs. But, with the knowledge of the directly observable internal conversion lifetime between these two states (~20 fs), the experimentally observed lifetimes can be refined using a simple sequential kinetic model (see Supplementary section S2.2).[42] Based on such a model, conservative estimates show that the $^2B_{3u}$ lifetime is < 30 fs and the

^2A_u lifetime is < 27 fs. The latter is in excellent agreement with the inferred lifetime of 25 fs from the spectral linewidth of this resonance (assuming homogeneous broadening). [12] It should be stressed that these observed lifetimes contain contributions from both internal conversion (τ_{ic}) and autodetachment (τ_{ad}) and the lifetimes for the individual decay channels will be longer: $(\tau_{obs})^{-1} = (\tau_{ic})^{-1} + (\tau_{ad})^{-1}$. For the $^2B_{3u}$ state, some insight can be gained into the lifetimes of autodetachment versus internal conversion based on the 3.10 eV PE spectrum, as it provides some information about the asymptotic product yields (see Supplementary section S2.2). Based on our assignment, the feature at *eKE* ~ 0.4 eV and the thermionic emission feature necessarily arise from internal conversion. Conversely, the feature at ~ 1.0 eV arises from a combination of direct and autodetachment. The ratio of these features suggests that at the very least 75% of population in the $^2B_{3u}$ undergoes internal conversion. Using this, the lifetime for internal conversion and autodetachment can be determined to be $\tau_{ic} < 40$ fs and $\tau_{ad} > 120$ fs, respectively (based on an observed lifetime of 30 fs). This observation complements the fact that the $^2B_{3u}$ state has been calculated to be predominantly a Feshbach-resonance, requiring a 2-electron transition to access the neutral ground state by autodetachment. [12,41] A similar disentanglement of the parallel dynamics is not possible for the ^2A_u state. The ^2A_u state is a shape-resonance and is expected to undergo much more rapid autodetachment than the $^2B_{3u}$ state. Nevertheless, internal conversion clearly can compete as evidenced by the strong thermionic emission signal in the PE spectra shown in Figure 1d. The extremely short internal conversion lifetimes of the excited states are consistent with the fact that the primary decay modes are coincident with the funnelling modes at the $^2B_{3u}/^2A_u$ and $^2A_u/^2B_{2u}$ intersections. The calculated frequencies for these C=C and C=O stretches range between 1600 cm^{-1} and 1800 cm^{-1}, which corresponds to a timescale of approximately 20 fs, in good agreement with the experimental observations.

Relevance to electron transfer

We now return to the relevance of our observations to the general electron accepting ability of pBQ and quinones. Our calculations show that the neutral pBQ ground state is nested in the excited state potentials of the radical anion. In this situation, Jortner's energy gap law[43] implies that electron attachment to the excited states is more favourable than to the ground state because the FC factors are higher. This supports the importance of the excited states for the electron accepting ability of pBQ. The geometry of the ^1A_g ground state of pBQ is in fact quite close to the FC geometry accessed in our optical excitation experiments of the radical anion. One may therefore expect similar initial excited state dynamics after electron attachment to those taking place after optical excitation, which involves primarily the C=O and C=C symmetric stretches. As a result, the excited states provide an alternative reaction pathway, bypassing the free energy barrier connecting the reactants to the products. Once these excited states are populated, extremely fast internal conversion drives the system towards the ground anionic state, preventing the back-electron transfer from occurring and quenching the highly reactive excited states. This alternative pathway preserves the overall driving force of the reaction, while avoiding the free energy barrier. In a condensed phase environment, any excess vibrational energy can be lost to the surroundings.

The excited states in 2,3,5,6-tetrafluoro-7,7,8,8-tetracyanoquinodimethane and the chloranil radical anions have also recently been studied. [44-47] In these related systems, the excited states similarly exhibit extremely short lifetimes on the order of 100 fs, although they are bound with respect to electron loss. The prevalent rapid dynamics observed in these quinoid systems suggest that the radical anion of pBQ dominates the electronic relaxation and can be thought of as an electrophore, in analogy to a chromophore. Conical intersections similar to those indentified here in the electrophore may account for the efficient internal conversion observed in molecular systems derived from it. In the context of ET in condensed phases or biological complexes, the above gas-phase picture is incomplete and the extended

environment must be taken into account. In strongly stabilising environments, the resonances may become bound. The generalised solvent coordinate shown in Figure 1a accounts for the response of the environment to the ET. Nevertheless, the bottom-up view presented here for pBQ provides a clear understanding of how excited states may participate in ET processes involving pBQ derivatives: the higher excited states of the anion act to capture the electron, while lower-lying states have the function of stabilising the electron.

Conclusion

The dynamics of excited states of $pBQ^{\bullet -}$ that are unbound with respect to autodetachment by >1.2 eV have been studied using a combination of time-resolved photoelectron spectroscopy and *ab initio* calculations. We show that internal conversion can compete effectively with autodetachment and proceeds through a series of electronically excited states. These are connected through conical intersections requiring totally symmetric stretches of the C=O and C=C bonds. From an electron acceptor viewpoint, pBQ serves as an ideal electrophore for highly exergonic electron transfer reactions due to a high density of states above threshold and an extremely efficient pathway to forming ground state products, which together provide a bypass to the free energy barrier in the Marcus inverted region.

Methods

Experimental methodology

Experiments were conducted using our femtosecond anion photoelectron imaging spectrometer, which has been described in detail previously. [46,48] It combines an electrospray ionisation source for the production of anions with velocity-map imaging. [49] Anions were produced by electrospraying a 20 mM solution of p-benzoquinone (98% Sigma-Aldrich) in acetonitrile at –2.5 kV and transferred into vacuum. Ions were accumulated and packets ejected at 500 Hz repetition rate into a collinear time-of-flight mass-spectrometer. The $pBQ^{\bullet -}$ ion packet was intersected in the centre of a velocity-map imaging setup by femtosecond pump and probe laser pulses. Detached photoelectrons were directed onto a position sensitive detector and PE images typically collected for 3×10^5 lasers shots per pump-probe delay. Raw images were deconvoluted using the polar onion-peeling algorithm. [50] PE spectra have been normalised relative to the $pBQ^{\bullet -}$ ion current. An energy resolution of $\Delta eKE/eKE \sim 5\%$ is achieved, calibrated to the well-known spectrum of iodide.

Femtosecond laser pulses were derived from a commercial Ti:Sapphire oscillator and amplifier laser. Pulses at 2.58 eV (480 nm) were generated by optical parametric conversion and subsequent frequency mixing with the fundamental, yielding ~100 μJ pulse energy. Pulses at 3.10 eV (400 nm) were generated through second harmonic generation in a type II beta-barium borate (BBO) crystal. 1.55 eV (800 nm) probe pulses were attenuated to 200 μJ per pulse. Pump and probe beams were combined collinearly before being loosely focused into the interaction region. The beam diameter at the interaction point is ~0.5 mm, corresponding to average power densities on the order of 2×10^{11} W cm^{-2}. Pump and probe pulses were delayed with respect to each other by a motorised optical delay line. The time-resolution of our experiments was limited by the cross-correlation of pump and probe pulses, which was measured inside a type II BBO non-linear crystal and was 65 fs.

Computational methodology

The potential energy surface calculations were carried out with the CASPT2//CASSCF approach, where critical points (minima and conical intersections) were optimized at the complete active space self-consistent field (CASSCF) level, and the energies were recalculated at the complete active space second-order perturbation theory (CASPT2) level to account for dynamic correlation. The aug-cc-pvdz basis set was used for CASSCF optimizations and the ANO-L basis set (contracted to C,O[4s3p2d1f]/H[3s2p1d]) was employed for CASPT2 calculations. The CASSCF calculations have been carried out with Gaussian 09 A.02, [51] and the CASPT2 calculations with Molcas7.2. [52] Computational details can be found in Supplementary section S3.

Acknowledgements

This work was funded by the EPSRC (EP/D073472/1), the Spanish Ministerio de Ciencia e Innovación (MICINN) (CTQ2011-26573 and UNGI08-4E-003 from FEDER (European Fund for Regional Development)), and the Catalan Agència de Gestió d'Ajuts Universitaris i de Recerca (SGR0528). Q. Li acknowledges a Juan de la Cierva fellowship of the MICINN. JRRV thanks the ERC for a Starting Grant. Correspondence and requests for materials should be addressed to LB or JRRV.

Author Contributions

DAH and QL contributed equally to this work. DAH and JRRV conceived the project and performed all the experiments. QL and LB designed and performed all the calculations. QL and DAH analysed the computational and experimental results. All authors discussed results and contributed to the manuscript.

Financial

The authors declare no competing financial interests.

References

1 El-Najjar, N. *et al.* The chemical and biological activities of quinones: overview and implications in analytical detection. *Photochem. Rev.* **10**, 353 (2011).

2 Nohl, H., Jordan, W. & Youngman, R. J. Quinones in Biology: Functions in electron transfer and oxygen activation. *Adv. Free Radical. Bio.* **2**, 211 (1986).

3 Iverson, T. M., Luna-Chavez, C. s., Cecchini, G. & Rees, D. C. Structure of the Escherichia coli Fumarate Reductase Respiratory Complex. *Science* **284**, 1961 (1999).

4 Marcus, R. A. & Sutin, N. Electron Transfers in Chemistry and Biology. *Biochim. Biophys. Acta* **811**, 265 (1985).

5 Rehm, D. & Weller, A. Kinetics and Mechanics of Electron Transfer during Fluorescence Quenching in Acetonitrile. *Ber. Bunsen-Ges. Phys. Chem.* **73**, 834 (1969).

6 Rehm, D. & Weller, A. Kinetics of Fluorescence Quenching by Electron and H-Atom Transfer. *Isr. J. Chem.* **8**, 259 (1970).

7 Calcaterra, L. T., Closs, G. L. & Miller, J. R. Fast intramolecular electron transfer in radical ions over long distances across rigid saturated hydrocarbon spacers. *J. Am. Chem. Soc.* **105**, 670 (1983).

8 Closs, G. L., Calcaterra, L. T., Green, N. J., Penfield, K. W. & Miller, J. R. Distance, stereoelectronic effects, and the Marcus inverted region in intramolecular electron transfer in organic radical anions. *J. Phys. Chem.* **90**, 3673 (1986).

9 Indelli, M. T., Ballardini, R. & Scandola, F. Experimental investigation of highly exergonic outer-sphere electron-transfer reactions. *J. Phys. Chem.* **88**, 2547 (1984).

10 Miller, J. R., Calcaterra, L. T. & Closs, G. L. Intramolecular long-distance electron transfer in radical anions. The effects of free energy and solvent on the reaction rates. *J. Am. Chem. Soc.* **106**, 3047 (1984).

11 Closs, G. L. & Miller, J. R. Intramolecular Long-Distance Electron-Transfer in Organic-Molecules. *Science* **240**, 440 (1988).

12 Schiedt, J. & Weinkauf, R. Resonant photodetachment via shape and Feshbach resonances: p-benzoquinone anions as a model system. *J. Chem. Phys.* **110**, 304 (1999).

13 Barbara, P. F., Meyer, T. J. & Ratner, M. A. Contemporary Issues in Electron Transfer Research. *J. Phys. Chem.* **100**, 13148 (1996).

14 Marcus, R. A. & Siders, P. Theory of highly exothermic electron transfer reactions. *J. Phys. Chem.* **86**, 622 (1982).

15 Mataga, N., Chosrowjan, H. & Taniguchi, S. Ultrafast charge transfer in excited electronic states and investigations into fundamental problems of exciplex chemistry: Our early studies and recent developments. *J. Photochem. Photobiol., C* **6**, 37 (2005).

16 Morandeira, A., Engeli, L. & Vauthey, E. Ultrafast Charge Recombination of Photogenerated Ion Pairs to an Electronic Excited State. *J. Phys. Chem. A* **106**, 4833 (2002).

17 Petersson, J., Eklund, M., Davidsson, J. & Hammarström, L. Ultrafast Electron Transfer Dynamics of a Zn(II)porphyrin-Viologen Complex Revisited: S2 vs S1 Reactions and Survival of Excess Excitation Energy. *J. Phys. Chem. B* **114**, 14329 (2010).

18 Weber, J., Malsch, K. & Hohlneicher, G. Excited electronic states of p-benzoquinone. *Chem. Phys.* **264**, 275 (2001).

19 El Ghazaly, M. O. A., Svendsen, A., Bluhme, H., Nielsen, S. B. Ø. & Andersen, L. H. Electron scattering on p-benzoquinone anions. *Chem. Phys. Lett.* **405**, 278 (2005).

20 Siegert, S., Vogeler, F. & Weinkauf, R. Direct Access to the Dipole-Forbidden nπ* T1 State of p-Benzoquinone by Photodetachment Photoelectron Spectroscopy. *Z. Phys. Chem. (Muenchen, Ger.)* **225**, 507 (2011).

21 Mariam, Y. H. & Chantranupong, L. Electron affinities of p-benzoquinone, p-benzoquinone imine and p-benzoquinone diimine, and spin densities of their p-benzosemiq. *J. Comput.-Aided Mol. Des.* **11**, 345 (1997).

22 Mohandas, P. & Umapathy, S. Density-Functional Studies on the Structure and Vibrational Spectra of Transient Intermediates of p-Benzoquinone. *J. Phys. Chem. A* **101**, 4449 (1997).

23 Pou-Amérigo, R., Serrano-Andrés, L., Merchán, M., Ortí, E. & Forsberg, N. A Theoretical Determination of the Low-lying Electronic States of the p-Benzosemiquinone Radical Anion. *J. Am. Chem. Soc.* **122**, 6067 (2000).

24 Honda, Y., Hada, M., Ehara, M. & Nakatsuji, H. Excited and Ionized States of p-Benzoquinone and Its Anion Radical: SAC-CI Theoretical Study. *J. Phys. Chem. A* **106**, 3838 (2002).

25 Fu, Q., Yang, J. & Wang, X.-B. On the Electronic Structures and Electron Affinities of the m-Benzoquinone (BQ) Diradical and the o-, p-BQ Molecules: A Synergetic Photoelectron Spectroscopic and Theoretical Study. *J. Phys. Chem. A* **115**, 3201 (2011).

26 Christophorou, L. G., Carter, J. G. & Christodoulides, A. A. Long-lived parent negative ions in p-benzoquinone formed by electron capture in the field of the ground and excited states. *Chem. Phys. Lett.* **3**, 237 (1969).

27 Collins, P. M., Christophorou, L. G., Chaney, E. L. & Carter, J. G. Energy dependence of the electron attachment cross section and the transient negative ion lifetime for p-benzoquinone and 1,4-naphthoquinone. *Chem. Phys. Lett.* **4**, 646 (1970).

28 Cooper, C. D., Naff, W. T. & Compton, R. N. Negative ion properties of p-benzoquinone: Electron affinity and compound states. *J. Chem. Phys.* **63**, 2752 (1975).

29 Suzuki, T. Femtosecond Time-Resolved Photoelectron Imaging. *Annu. Rev. Phys. Chem.* **57**, 555 (2006).

30 Verlet, J. R. R. Femtosecond spectroscopy of cluster anions: insights into condensed-phase phenomena from the gas-phase. *Chem. Soc. Rev.* **37**, 505 (2008).

31 Ghigo, G., Roos, B. O. & Malmqvist, P.-Å. A modified definition of the zeroth-order Hamiltonian in multiconfigurational perturbation theory (CASPT2). *Chem. Phys. Lett.* **396**, 142 (2004).

32 Pegg, D. J. Structure and dynamics of negative ions. *Rep. Prog. Phys.* **67**, 857 (2004).

33 Wigner, E. P. On the Behavior of Cross Sections Near Thresholds. *Phys. Rev.* **73**, 1002 (1948).

34 Baguenard, B., Pinaré, J. C., Bordas, C. & Broyer, M. Photoelectron imaging spectroscopy of small tungsten clusters: Direct observation of thermionic emission. *Phys. Rev. A* **63**, 023204 (2001).

35 Hansen, K., Hoffmann, K. & Campbell, E. E. B. Thermal electron emission from the hot electronic subsystem of vibrationally cold C60. *J. Chem. Phys.* **119**, 2513 (2003).

36 Horke, D. A. & Verlet, J. R. R. Photoelectron spectroscopy of the model GFP chromophore anion. *Phys. Chem. Chem. Phys.* **14**, 8511-8515 (2012).

37 Bernardi, F., Olivucci, M. & Robb, M. A. Potential energy surface crossings in organic photochemistry. *Chemical Society Reviews* **25**, 321-&, doi:10.1039/cs9962500321 (1996).

38 Domcke, W., Yarkony, D. R. & Köppel, H. *Conical Intersections: Electronic Structure, Dynamics & Spectroscopy.*, (World Scientific: Singapore, 2004).

39 Klessinger, M. & Michl, J. *Excited States and Photochemistry of Organic Molecules*. (VCH Publishers, Inc.: New York, 1995).

40 Yarkony, D. R. Conical intersections: The new conventional wisdom. *Journal of Physical Chemistry A* **105**, 6277-6293, doi:10.1021/jp00373lu (2001).

41 Simons, J. in *Resonances* Vol. 263 *ACS Symposium Series* 3 (American Chemical Society, 1984).

42 Verlet, J. R. R., Bragg, A. E., Kammrath, A., Cheshnovsky, O. & Neumark, D. M. Time-resolved relaxation dynamics of Hg[sub n][sup -] (11 <= n <= 16,n = 18) clusters following intraband excitation at 1.5 eV. *J. Chem. Phys.* **121**, 10015 (2004).

43 Ulstrup, J. & Jortner, J. The effect of intramolecular quantum modes on free energy relationships for electron transfer reactions. *The Journal of Chemical Physics* **63**, 4358-4368 (1975).

44 Horke, D. A., Roberts, G. M. & Verlet, J. R. R. Excited States in Electron-Transfer Reaction Products: Ultrafast Relaxation Dynamics of an Isolated Acceptor Radical Anion. *J. Phys. Chem. A* **115**, 8369 (2011).

45 Horke, D. A. & Verlet, J. R. R. Time-resolved photoelectron imaging of the chloranil radical anion: ultrafast relaxation of electronically excited electron acceptor states. *Phys. Chem. Chem. Phys.* **13**, 19546 (2011).

46 Lecointre, J., Roberts, G. M., Horke, D. A. & Verlet, J. R. R. Ultrafast Relaxation Dynamics Observed Through Time-Resolved Photoelectron Angular Distributions. *J. Phys. Chem. A* **114**, 11216 (2010).

47 Roberts, G. M., Lecointre, J., Horke, D. A. & Verlet, J. R. R. Spectroscopy and dynamics of the 7,7,8,8-tetracyanoquinodimethane radical anion. *Phys. Chem. Chem. Phys.* **12**, 6226 (2010).

48 Horke, D. A., Roberts, G. M., Lecointre, J. & Verlet, J. R. R. Velocity-map imaging at low extraction fields. *Rev. Sci. Instrum.* **83**, 063101 (2012).

49 Eppink, A. T. J. B. & Parker, D. H. Velocity map imaging of ions and electrons using electrostatic lenses: Application in photoelectron and photofragment ion imaging of molecular oxygen. *Rev. Sci. Instrum.* **68**, 3477 (1997).

50 Roberts, G. M., Nixon, J. L., Lecointre, J., Wrede, E. & Verlet, J. R. R. Toward real-time charged-particle image reconstruction using polar onion-peeling. *Rev. Sci. Instrum.* **80**, 053104 (2009).

51 Frisch, M. J. *et al.* Gaussian, Inc., Wallingford CT (2009).

52 Karlström, G. *et al.* MOLCAS: a program package for computational chemistry. *Comp. Mater. Sci.* **28**, 222 (2003).

Table 1. CASPT2 energies [eV] of the five lowest doublet states and the lowest singlet at the relevant structures of the potential energy surface.[a,b]

Structure	$E(D_0)$	$E(D_1)$	$E(D_2)$	$E(D_3)$	$E(D_4)$	$E(S_0)$
$(^2B_{2g})_{min}$[c]	**0.00** ($^2B_{2g}$)	2.29 ($^2B_{2u}$) (< 0.001)	2.37 ($^2B_{3g}$) (<0.001)	2.58 (^2A_u) (0.089)	3.13 ($^2B_{3u}$) (0.090)	2.20 (^1A_g)
$(^2B_{3u})_{min}$	0.15 ($^2B_{2g}$)	2.00 ($^2B_{2u}$)	2.17 ($^2B_{3g}$)	**2.78** ($^2B_{3u}$)	2.81 (^2A_u)	2.75 (^1A_g)
$(^2A_u)_{min}$	0.25 ($^2B_{2g}$)	**2.47** (^2A_u)	2.60 ($^2B_{2u}$)	2.69 ($^2B_{3g}$)	3.41 ($^2B_{3u}$)	2.18 (^1A_g)
$(^2B_{2u})_{min}$	0.19 ($^2B_{2g}$)	**2.03** ($^2B_{2u}$)	2.17 ($^2B_{3g}$)	2.84 ($^2B_{3u}$)	2.94 (^2A_u)	2.73 (^1A_g)
$(^2B_{2g}/^2A_u)_X$	**2.79** ($^2B_{2g}$)	**2.94** (^2A_u)	5.82 ($^2B_{2u}$)	5.87 ($^2B_{3g}$)	5.94 ($^2B_{3u}$)	4.05 (^1A_g)
$(^2B_{2g}/^2B_{3u})_X$	**2.94** ($^2B_{2g}$)	**3.26** ($^2B_{3u}$)	5.20 (^2A_u)	6.02 ($^2B_{3g}$)	6.07 ($^2B_{2u}$)	3.97 (^1A_g)
$(^1A_g)_{min}$	0.31 ($^2B_{2g}$)	2.65 ($^2B_{3u}$)	2.92 ($^2B_{2u}$)	2.96 ($^2B_{3g}$)	3.71 ($^2B_{3u}$)	**2.04** (^1A_g)[d]

[a]State symmetry in brackets. Dominant electronic configuration referred to the orbitals of Figure 1e: $^2B_{2g}$: $(4b_{3g})^2(5b_{2u})^2(2b_{3u})^2(2b_{2g})^1$; $^2B_{2u}$: $(4b_{3g})^2(5b_{2u})^1(2b_{3u})^2(2b_{2g})^2$; $^2B_{3g}$: $(4b_{3g})^1(5b_{2u})^2(2b_{3u})^2(2b_{2g})^2$; ^2A_u: $(4b_{3g})^2(5b_{2u})^2(2b_{3u})^2(1a_u)^1$; $^2B_{3u}$: $(4b_{3g})^2(5b_{2u})^2(2b_{3u})^1(2b_{2g})^2$; ^1A_g: $(4b_{3g})^2(5b_{2u})^2(2b_{3u})^2$. [b]Energy of the optimised state (adiabatic excitation energies for the $^2B_{3u}$, ^2A_u and $^2B_{2u}$ states) in bold characters. [c]Energies correspond to vertical excitations of the quinone anion; oscillator strength in brackets. [d]Corresponds to the adiabatic electron affinity.

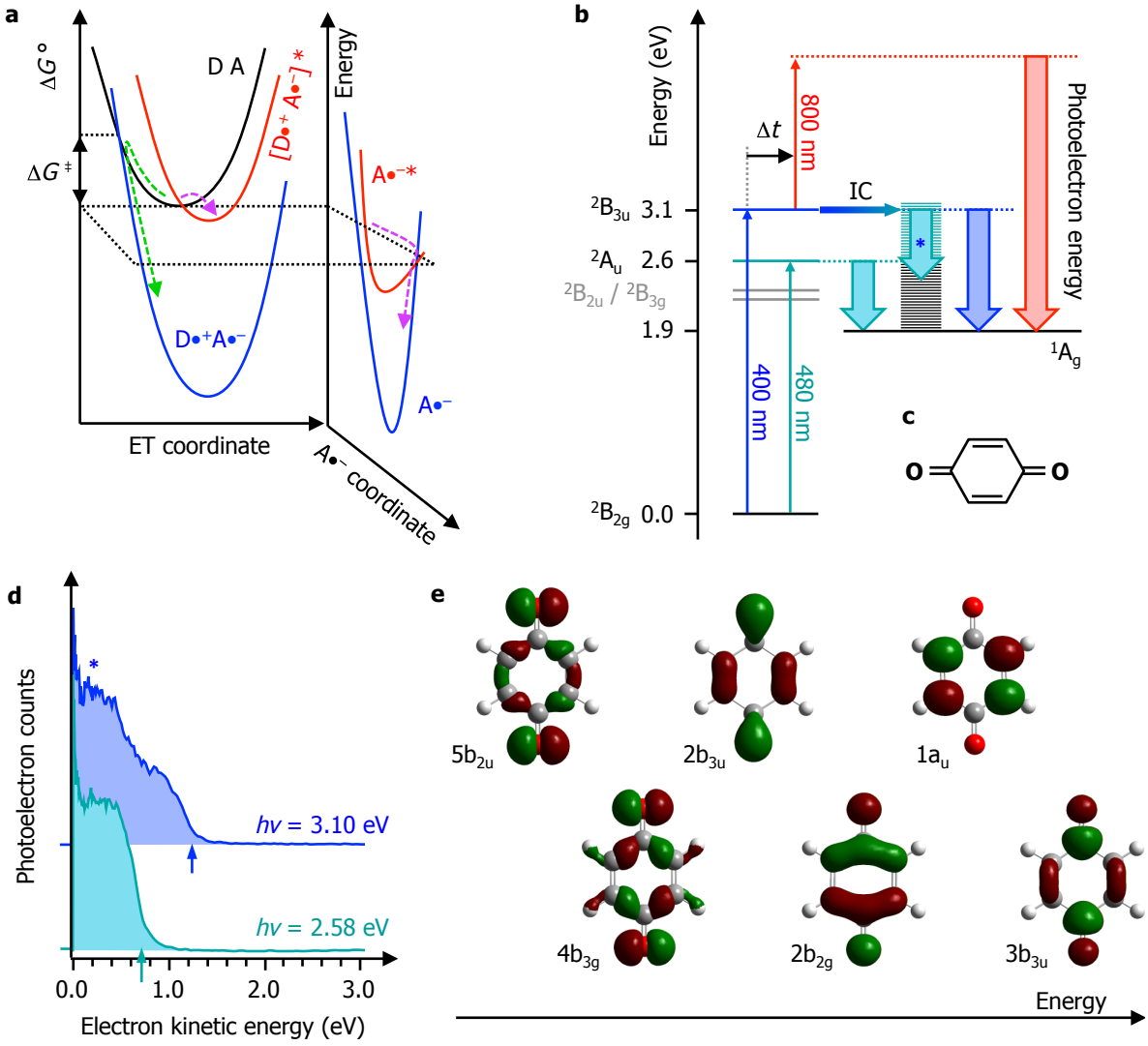

Figure 1 | Overview of electron transfer reactions and electronic structure of parabenzoquinone. a, schematic diagram of the free energy profile along an exergonic electron transfer reaction coordinate (green arrow) from DA to D•$^{+}$A•$^{-}$. The reaction path forming excited states of the products, [D•$^{+}$ A•$^{-}$]*, shown in purple, provides a lower activation barrier. These excited states can relax via the internal coordinates of A•$^{-}$ as shown. **b**, energy level diagram for A•$^{-}$ = pBQ•$^{-}$ indicating all relevant electronic states. Downward arrows schematically represent the energy of the emitted photoelectrons. Also shown is the pump-probe scheme involving delayed detachment using 1.55 eV (800 nm) probe pulses. **c**, structure of pBQ. **d**, photoelectron spectra of pBQ•$^{-}$ for the excitation processes shown in **b**. The asterisk highlights photoelectrons emitted around 0.4 eV in the 3.10 eV spectrum that are arising from the internal conversion (IC) from the $^{2}B_{3u}$ state to the $^{2}A_{u}$ state, which then autodetaches as shown in **b**. The maximum kinetic energy is indicated by upward pointing arrow. **e**, relevant molecular orbitals of pBQ•$^{-}$, shown in increasing energy from left to right.

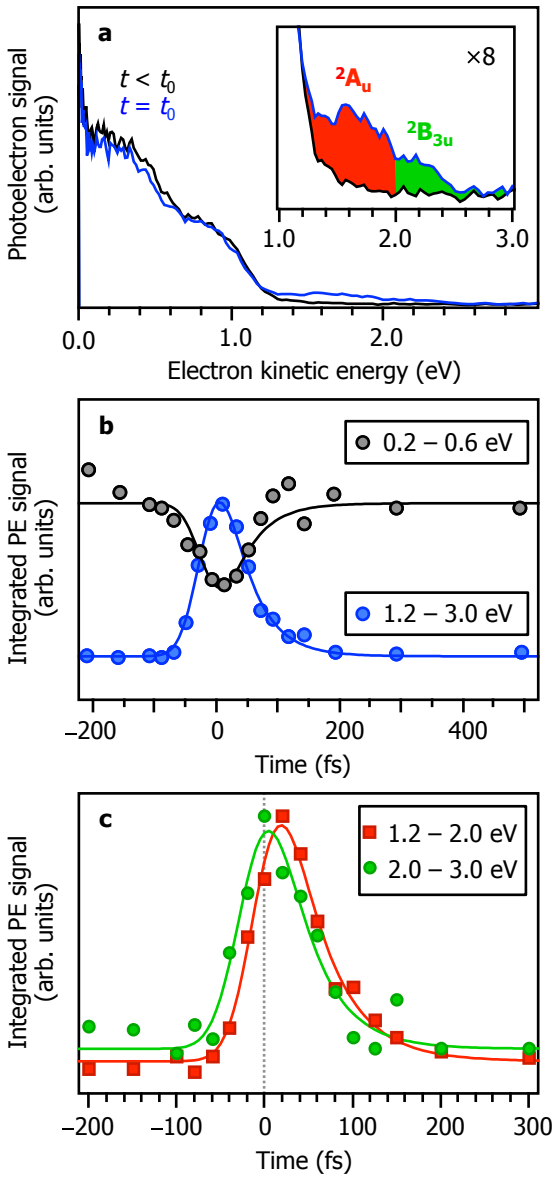

Figure 2 | Excited state dynamics of above-threshold states. **a**, time-resolved photoelectron spectra taken with 3.10 eV (400 nm) pump and 1.55 eV (800 nm) probe. At the temporal overlap ($t = t_0$), a new feature is seen at high electron kinetic energy (see Figure 1**b** for excitation scheme), while the low energy feature is depleted. The inset highlights the high energy pump-probe feature, in which the red and green shading can be assigned to the probing of the ^2A_u and $^2B_{3u}$ excited states, respectively. **b**, photoelectron signal integrated over spectral regions indicated, showing the excited state decay and depletion recovery. **c**, photoelectron signal integrated over spectral regions corresponding to the ^2A_u (red) and $^2B_{3u}$ (green) excited states, demonstrating that there is a ~20 fs delay in the appearance of the ^2A_u signal that can be assigned to internal conversion from the initially excited $^2B_{3u}$ state.

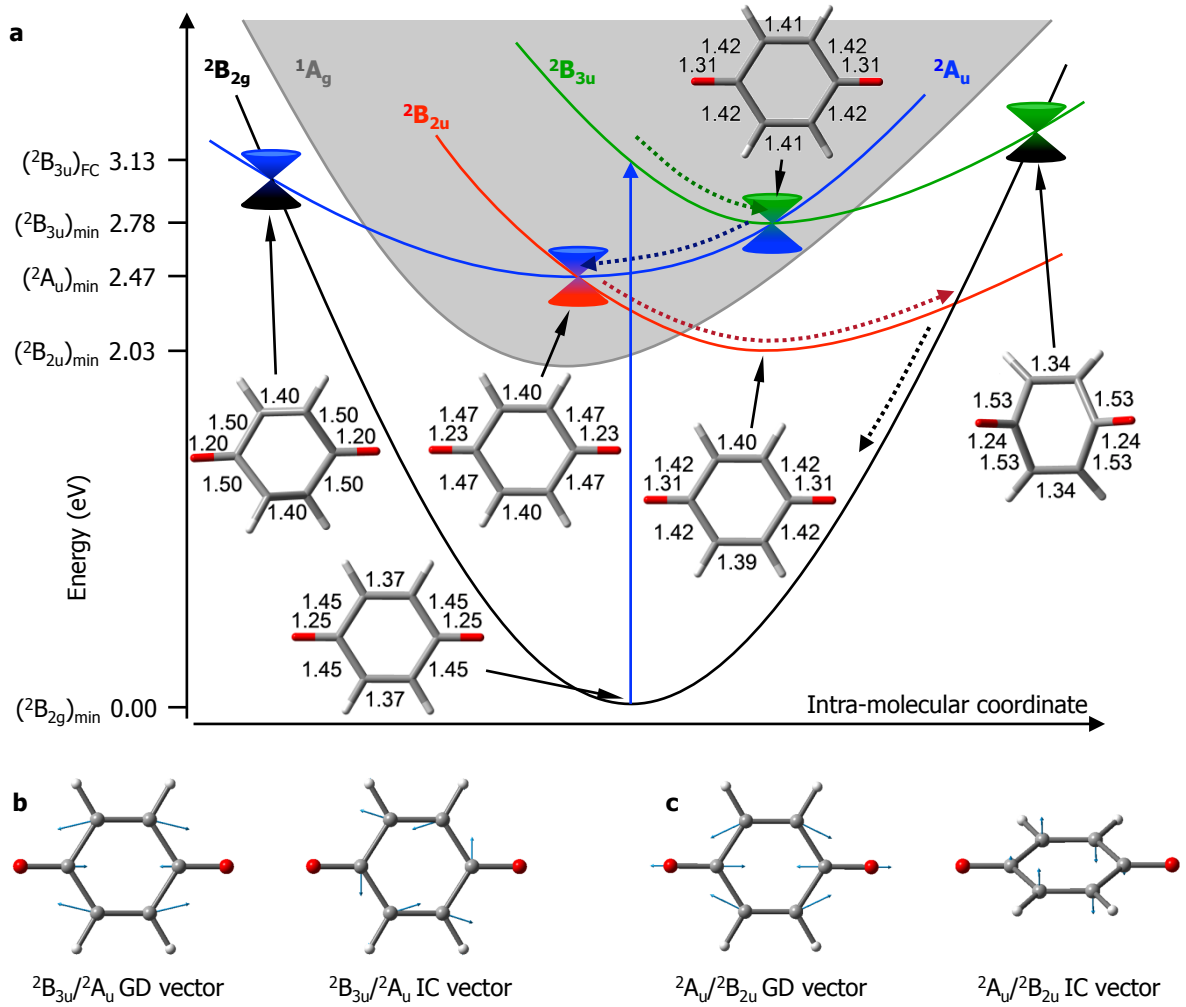

Figure 3 | Mechanistic picture of electron stabilisation. **a**, potential energy diagram showing the excited state dynamics leading to ultrafast decay of pBQ•⁻. The grey shaded area indicates the unbound energy levels of the anion. Initial excitation to the $^2B_{3u}$ state leads to a conical intersection with the ^2A_u state, which in turn intersects with the $^2B_{2u}$ state, before becoming bound with respect to electron detachment and internally converting to the ground $^2B_{2g}$ state. The $^2B_{3g}$ state has been omitted for clarity but may play a role in the dynamics from the $^2B_{2u}$ state internal conversion to form the ground state. The geometries at key points along the decay path are shown. Alternative routes are also shown but require large out-of-plane motion. **b** and **c**, gradient difference (GD) and the interstate coupling (IC) vectors for the conical intersection between the $^2B_{3u}$ and ^2A_u states and the ^2A_u and $^2B_{2u}$ states, respectively.